NASA TECHNICAL NOTE

NASA TN D-6927

NASA TN D-6927

MEASURED AND CALCULATED MEAN-FLOW PROPERTIES OF A TWO-DIMENSIONAL, HYPERSONIC, TURBULENT WAKE

by Richard D. Wagner

Langley Research Center
Hampton, Va. 23365

NATIONAL AERONAUTICS AND SPACE ADMINISTRATION • WASHINGTON, D. C. • NOVEMBER 1972

1. Report No.	2. Government Accession No.	3. Recipient's Catalog No.
NASA TN D-6927		

4. Title and Subtitle	5. Report Date
MEASURED AND CALCULATED MEAN-FLOW PROPERTIES OF A TWO-DIMENSIONAL, HYPERSONIC, TURBULENT WAKE	November 1972
	6. Performing Organization Code

7. Author(s)	8. Performing Organization Report No.
Richard D. Wagner	L-8158
	10. Work Unit No.
9. Performing Organization Name and Address	501-06-08-01
NASA Langley Research Center Hampton, Va. 23365	11. Contract or Grant No.
	13. Type of Report and Period Covered
12. Sponsoring Agency Name and Address	Technical Note
National Aeronautics and Space Administration Washington, D.C. 20546	14. Sponsoring Agency Code

15. Supplementary Notes

16. Abstract

The hypersonic turbulent wake produced by a wedge was studied experimentally and its properties were compared with predictions obtained from a numerical computation procedure. In the computation procedure several models for the eddy-viscosity formulation of the turbulent transport were examined. Conventional-defect models and a modified mixing-length model were found to yield good predictions of the experimental data. The classical mixing-length model gave unrealistic results. The experimental data displayed similarity when velocity and temperature defects were scaled by the maximum defects and the transverse coordinate was scaled by the velocity-defect half-width.

17. Key Words (Suggested by Author(s))	18. Distribution Statement
Hypersonic turbulent wake Experimental data Numerical computations Shear flow Turbulent flow	Unclassified – Unlimited

19. Security Classif. (of this report)	20. Security Classif. (of this page)	21. No. of Pages	22. Price*
Unclassified	Unclassified	33	$3.00

*For sale by the National Technical Information Service, Springfield, Virginia 22151

MEASURED AND CALCULATED MEAN-FLOW PROPERTIES OF A TWO-DIMENSIONAL, HYPERSONIC, TURBULENT WAKE

By Richard D. Wagner
Langley Research Center

SUMMARY

The hypersonic turbulent wake produced by a wedge was studied experimentally and its properties were compared with predictions obtained from a numerical computation procedure. In the computation procedure several models for the eddy-viscosity formulation of the turbulent transport were examined. Conventional-defect models and a modified mixing-length model were found to yield good predictions of the experimental data. The classical mixing-length model gave unrealistic results. The experimental data displayed similarity when velocity and temperature defects were scaled by the maximum defects and the transverse coordinate was scaled by the velocity-defect half-width.

INTRODUCTION

Current interest in hypersonic turbulent shear flows stems from several practical problems requiring knowledge of the flow properties in such free shear layers. One such problem is the use of vehicle wake observables for entry-vehicle discrimination (ref. 1); another is determining the effects of impingement of a free shear layer on the surface of a hypersonic vehicle. These shear layers are often produced by the interaction of shocks from components of the vehicle (ref. 2). Each of these problems is characterized by a close coupling of the developing time-averaged mean flow and the flow turbulence.

At present, numerical techniques exist which compute turbulent shear flows with phenomenological models for the turbulent transport. Usually, these models for hypersonic turbulent free shear layers are seemingly logical extensions of models which have given reasonable results in comparisons with low-speed experimental data. However, experiments are needed to assess the applicability of these extensions to the hypersonic turbulent shear layer.

The present paper reports the results of experiments conducted in the Langley 22-inch helium tunnel to determine flow characteristics in the turbulent wake produced by a 45° total-angle wedge. The measurements made include tests to ascertain the turbulent character of the wake, and surveys of the wake pitot pressure, total temperature,

and static pressure. Experimental data at an initial station are used to start computations of the subsequent wake development by inserting various turbulent transport models into a numerical computation procedure. The data downstream of the initial station are compared with computed distributions of flow properties at several stations in the wake.

SYMBOLS

$C = \rho\mu$

C_γ	constant in intermittency distribution
c_p	specific heat at constant pressure
d	diameter of static probe
h	static enthalpy
j	equal to 0 for two-dimensional flow and 1 for axisymmetric flow
K_m, K_u	constants in eddy-viscosity formulation (eqs. (12) and (13))
k	thermal conductivity
l	mixing length
l_1	constant in mixing-length formulation
M	Mach number
p	static pressure
p_{or}	orifice static pressure
p_t	stagnation pressure
$p_{t,2}$	pitot pressure
R	local Reynolds number

R_T	turbulent Reynolds number
R_{tr}	transition Reynolds number
R_∞	free-stream Reynolds number based on wedge thickness, $\frac{\rho_\infty u_\infty t}{\mu_\infty}$
r_b	characteristic body dimension; $r_b = t$ for two-dimensional body
T	static temperature
T_{aw}	adiabatic wall temperature
T_t	total temperature
t	wedge base thickness
u,v	velocity components in x- and y-directions
x,y,z	Cartesian coordinates (fig. 1)
$y_{1/2}$	half-width for velocity defect
γ	ratio of specific heats
γ_T	intermittency factor
δ	wake width
δ^*	displacement thickness
$\bar{\xi},\bar{\tau}$	transformed coordinates (eqs. (6))
θ	momentum thickness
θ_w	wedge half-angle
μ	viscosity
ρ	density

σ	Prandtl number
τ	Von Mises variable

Subscripts:

e	local wake-edge value
i	initial station
l	local value in wake, or laminar quantity
o	value at $y = 0$
sd	sticking distance
T	turbulent quantity
tr	at transition location
x,y	x or y partial derivative
$\bar{x},\bar{y}$	$\bar{x}$ or $\bar{y}$ partial derivative
$\bar{\zeta},\bar{\tau}$	$\bar{\zeta}$ or $\bar{\tau}$ partial derivative
∞	free-stream value

A bar over a symbol denotes a nondimensional quantity.

APPARATUS AND TESTS

Test Facility

The experiments were conducted in the Langley 22-inch helium tunnel. This blowdown-type tunnel has a contoured nozzle and a 0.559-meter-diameter test section. The free-stream Mach number in the test core is nearly constant at any given stagnation pressure (i.e., the axial and lateral Mach number gradients are negligible). A calibration and description of the facility are given in reference 3. For the present tests the stagnation pressure and temperature were 6.89×10^6 N/m^2 and 370 K, respectively. The

corresponding test-core Mach number was 20.4 and the unit Reynolds number was 1.34×10^7 per meter.

Model and Instrumentation

The wake was generated by a 45° total-angle wedge which had a base thickness of 2.54 cm and spanned the tunnel test section. (See fig. 1.) The wedge was constructed of fiber glass (Hetron 72 laminate) with an inlaid, stainless-steel, sharp leading edge. Five static-pressure orifices (0.23 cm in diameter) were placed in the base to measure base pressure.

A splitter plate could be attached to the base of the wedge to form a rearward-facing step with a depth equal to one-half of the base thickness. The plate was 0.46 meter long and spanned the base of the wedge. Fifteen static-pressure orifices, 0.23 cm in diameter, were placed along the midspan line of the plate and connected to capacitance-type pressure transducers.

Before each test the wedge surface was at room temperature. The stagnation temperature, 370 K, was selected so that room temperature would be near the adiabatic wall temperature for the flow over the windward surface of the wedge. A recovery factor at the model surface equal to the square root of the Prandtl number was assumed since the flow on the model was laminar; for the wedge-flow Mach number, 2.84, this value is near the exact value given by laminar theory. (See ref. 4.) Theoretical analyses for the recovery factor of the base flow are not available, and the adiabatic wall temperature on the base of the wedge may not equal room temperature. Nevertheless, the low heat-transfer coefficients with the small temperature potentials that are likely to exist should lead to negligible heat transfer in the base region. Thus, the present flow conditions may be assumed to be essentially adiabatic.

Surveys of wake flow properties were made at several chordwise stations behind the wedge. The survey rake is sketched in figure 1. The pitot tube was a 0.152-cm-diameter tube which was flattened to 0.102 cm across the flats; the tube was connected to a diaphragm-type pressure transducer located on the rake support inside the tunnel test section. The total-temperature probe was a shielded chromel-alumel thermocouple with an outside diameter of 0.094 cm. The third probe shown in figure 1 was a hot-wire probe connected to a constant-current anemometer with a frequency response of 100 kHz. The wire was tungsten, 3.56 micrometers in diameter and about 0.1 cm long. The hot wire was operated at a fixed current during the surveys, and only the rms of the voltage fluctuations from the compensating amplifier was monitored. The hot wire was used only to assist in detecting the character of the wake (i.e., whether laminar or turbulent).

During the 50-second run time available, the survey rake was moved across the wake at about 0.17 cm/sec. The probes started about 1 cm below the wake plane of symmetry (confirmed by the pitot-pressure symmetry) and traversed to about 7.6 cm above the plane of symmetry. The pitot tube moved in a plane passing through the model midspan, and the total-temperature and hot-wire probes translated in parallel planes, displaced 0.95 cm on either side of the pitot tube. Tests at fixed positions indicated that the speed of the probe response was sufficient to prevent errors due to the continuous probe movement.

Measurements of the low static pressures in the wake required the full test time available; hence, detailed surveys were not practical, and only the static pressure along the wake plane of symmetry was measured. The static-pressure probe was a 0.317-cm-diameter tube with a 17.7° half-angle cone tip. (See fig. 2.) A static-pressure orifice was located 5.33 cm from the cone tip. Inviscid pressure ratios (obtained from calculations by the inviscid method of characteristics) at the orifice as a function of Mach number are shown also in figure 2. For the present tests the local Mach number was always less than about 6, so that the inviscid pressure would be slightly less than the local static pressure ahead of the probe. The viscous effects on a static-pressure probe having a geometry similar to the present probe have been studied by Behrens. (See ref. 5.) Although Behrens' experiments on a 10° half-angle cone followed by a cylinder were in air, neither the effect of the present different forebody (17.7° half-angle cone) nor the effect of the different specific-heat ratios is believed to be large; thus, the calibration reported by Behrens should give a good estimate of the viscous effects on the present static-pressure probe. This estimate implies that the maximum viscous correction would be an increase of about 5 percent. That is, the measured pressure would be 5 percent greater than the inviscid pressure. In view of these offsetting differences, the present uncorrected static pressure might be expected to be close to the true static pressure ahead of the probe; further data to support this contention will be discussed subsequently.

RESULTS AND DISCUSSION

Survey Data

Schlieren and electron-beam photographs of the wake are shown in figure 3. The flow features, as identified in figure 3(c), are typical of those reported elsewhere in the literature. (See ref. 6.) Downstream of the base recirculation region and the wake neck, the flow is divided into three identifiable regions: The central viscous wake, the inviscid flow surrounding the viscous wake, and the inviscid flow above the wake shock.

Pitot-pressure and total-temperature profiles are shown in figures 4 and 5 for 10 positions behind the wedge. (The total-temperature probe was inoperative for the

survey at $x/t = 4$.) The profiles extended through the upper half of the viscous wake, the wake recompression shock, and part of the inviscid flow above the wake recompression shock. The spreading of the viscous wake and wake recompression shock is evident in both the pitot-pressure and total-temperature profiles. At the recompression shock, the total-temperature profiles show a decrease in T_t which could be due to a transient caused by the discontinuity in recovery temperature of the probe shield as it crosses the shock. Everywhere, the total temperature is either less than or equal to the free-stream total temperature. This effect is not understood since some increase above free-stream total temperature would be expected in view of the overshoot that would occur in the wedge boundary layer for adiabatic conditions.

The surveys did not extend all the way to the wedge bow shock since this flow region was not of primary interest; this flow should be simply that resulting from the centered expansion of the wedge flow and the interaction with the expansion waves reflected from the bow wave. The centered expansion of the wedge flow was verified by determining lines of constant pitot pressure in the flow above the recompression shock. (See fig. 6.) The center of the expansion (obtained by averaging over the intersections of pairs of linear curves fitted to the data by least-squares error) is located about four boundary-layer displacement thicknesses upstream of the base and slightly above the wedge boundary-layer edge. Theoretical analysis (ref. 7) gives a comparable distance for the upstream effect of a corner on an approaching laminar boundary layer. The upstream boundary layer "feels" the corner by propagation through the subsonic portion of the boundary layer. It should be noted that some error is introduced in the location of the expansion center since the region shown in figure 6 includes portions of the expansion fan influenced by bow-wave reflections. The limiting characteristic, the first wave of the expansion fan that is reflected from the bow wave, is shown to cross the lines of constant pitot pressure. (The limiting characteristic and the bow shock were calculated by an inviscid method of characteristics.) However, the local Mach number varies from about 6 on the first line of constant pitot pressure shown to about 10 on the last. At these high Mach numbers, one would not expect significant bending of the expansion-fan rays by the reflections.

The static-pressure distribution obtained along the wake plane of symmetry with the static-pressure probe is shown in figure 7 along with static pressures measured on a splitter plate attached to the model base. The pressures on the splitter plate show the recompression from the measured base pressure (an average of the nearly constant pressure indicated at the five static-pressure orifices without the splitter plate) in the wake neck region followed by a pressure decay farther downstream. Also shown is an exact calculation by the inviscid method of characteristics for a wedge followed by a flat plate (no rearward step). Beyond the recompression, the wake static pressure agrees with the calculated pressure and thus indicates that the recompression region has only a local effect on the inviscid-wake development. The greater displacement effect which would

occur on the splitter plate than in the wake must produce the higher pressures seen on the plate. One would expect the inviscid calculation to represent a lower bound on the static pressure, and certainly the splitter plate would be an upper bound. The close agreement of the measured and calculated wake static pressures gives further credence to the use of the direct measurements, as discussed earlier, for subsequent calculations of the viscous-wake flow properties.

The wake flow properties were computed from the survey data as follows. First, the static pressure was assumed to be constant across the viscous wake. (See ref. 8.) From the measured static and pitot pressure the local Mach number is found from normal-shock relations, and the velocity and static-temperature ratios were found by using (ref. 9)

$$\frac{u}{u_e} = \frac{M}{M_e}\sqrt{\frac{T_t}{T_{t,e}}\frac{1+\frac{\gamma-1}{2}M_e^2}{1+\frac{\gamma-1}{2}M^2}} \tag{1}$$

and

$$\frac{T}{T_e} = \frac{T_t}{T_{t,e}}\frac{1+\frac{\gamma-1}{2}M_e^2}{1+\frac{\gamma-1}{2}M^2} \tag{2}$$

Velocity and temperature ratios for $x/t \geq 6.0$ are given in table I along with the wake-edge conditions.

Transition Detection

The occurrence of transition and the existence of turbulent flow in the wake were determined by surveys with a constant-current hot-wire anemometer. The hot-wire rms voltage fluctuations across the viscous wake are shown in figure 8(a). In each profile the wake recompression shock appears as the region of large rms voltage outside the viscous wake; the locations of the high fluctuations agree with the location of the wake recompression shock found from schlieren photographs and shown in the figure. At $x/t = 1$, the hot-wire data show little turbulence in the viscous wake, but considerable turbulence develops between $x/t = 2$ and $x/t = 6$. Somewhere upstream of $x/t = 4$, an apparent increase of the turbulence (above the background level) at the middle of the wake is observed; according to the criterion used by Demetriades (ref. 10), an increase in the turbulence at the middle of the wake is indicative of transition to turbulent flow. At $x/t = 6$, the rms voltage profile shows considerable turbulence throughout the viscous

wake. Therefore, transition seems to occur at $x/t \approx 4$. A further check on the transition location uses a criterion put forth by Demetriades (ref. 11): that wake transition can be observed as a change in the x variation of the square of the reciprocal of the maximum velocity defect, that is, the defect at $y = 0$. This criterion also shows transition to occur around $x/t \approx 4$. (See fig. 8(b).) The wake transition Reynolds number

$$R_{tr} = \frac{\rho_e u_e}{\mu_e}\left(x_{tr} - x_{sd}\right)$$

would then be about 10^5 based on local flow conditions and assuming the "sticking distance" $\left(\text{the high Reynolds number upstream limit of the transition point } x_{sd}/t\right)$ to be about 1.

Demetriades' measurements of transition locations in the wakes of wedges at a free-stream Mach number of 6 (ref. 10) may be compared with this transition measurement. A local Reynolds number is more appropriate to compare the results of Demetriades for a free-stream Mach number of 6 with the present data for a free-stream Mach number of 20.4. There are two reasons for this: first, Batt (ref. 8), using local instead of free-stream conditions at $M = 6$ on a 20^o total-angle wedge, has found only a slight change in the transition Reynolds number, and second, the wake-edge Mach number for both the Demetriades data and the present data would be about 6. From reference 10 the transition sticking distance x_{sd} would be about 1.0 and the transition Reynolds number R_{tr} would be about 4×10^5, somewhat higher than observed herein. The lower transition Reynolds number in the present study could be due to the "unit Reynolds effect" observed in reference 12 and common to wind-tunnel boundary-layer transition studies (ref. 9), that is, the dependence of the transition location upon the facility free-stream disturbance level. In hypersonic tunnels the dominant source of free-stream disturbances is sound radiated by the turbulent nozzle-wall boundary layers (refs. 9 and 13). The sound level in the present tests would be much greater than in the lower Mach number studies owing to the rapid increase in sound intensity radiated from a turbulent boundary layer as Mach number increases (ref. 13).

Theoretical Predictions and Comparisons With Experiment

Theoretical calculations.- To compute the wake development from the initial input profiles, an implicit finite-difference method was used to solve the equations of motion. The method used was that developed and programed by Sinha, Fox, and Weinberger (ref. 14) but modified to account for pressure-gradient effects correctly. For flows having a streamwise pressure gradient, the continuity equation as formulated and programed in reference 14 is not satisfied by the nondimensional Von Mises transformation used in the analysis therein. (This becomes apparent when the continuity equation is nondimensionalized and expanded.) It should be pointed out that the same improper formulation is

used by Zakkay and Fox in reference 15. The proper formulation is given in the following equations. Only single-component, ideal gases are considered herein. The equations of motion are

Continuity:

$$\left.\begin{aligned} &\frac{\partial}{\partial x}\left(\rho u y^j\right) + \frac{\partial}{\partial y}\left(\rho v y^j\right) = 0 \\ &\text{Momentum:} \\ &\rho u \frac{\partial u}{\partial x} + \rho v \frac{\partial u}{\partial y} = -\frac{\partial p_e}{\partial x} + y^{-j} \frac{\partial}{\partial y}\left(\mu y^j \frac{\partial u}{\partial y}\right) \\ &\text{Energy:} \\ &\rho u c_p \frac{\partial T}{\partial x} + \rho v c_p \frac{\partial T}{\partial y} = u \frac{\partial p_e}{\partial x} + y^{-j} \frac{\partial}{\partial y}\left(k y^j \frac{\partial T}{\partial y}\right) + \mu\left(\frac{\partial u}{\partial y}\right)^2 \end{aligned}\right\} \tag{3}$$

where $j = 0$ or 1 for two-dimensional or axisymmetric flow, respectively.

By introducing a Von Mises transformation

$$\left.\begin{aligned} (1 + j)\tau^j \tau_y &= \rho u y^j \\ (1 + j)\tau^j \tau_x &= -\rho v y^j \end{aligned}\right\} \tag{4}$$

the continuity equation is satisfied, and the momentum and energy equations are

$$\left.\begin{aligned} &\rho u \frac{\partial u}{\partial x} = -\frac{\partial p_e}{\partial x} + \frac{\rho u}{(1 + j)^2} \tau^{-j} \frac{\partial}{\partial \tau}\left(\rho u \mu y^{2j} \tau^{-j} \frac{\partial u}{\partial \tau}\right) \\ &\text{and} \\ &\rho u c_p \frac{\partial T}{\partial x} = u \frac{\partial p_e}{\partial x} + \frac{\rho u \tau^{-j}}{(1 + j)^2} \frac{\partial}{\partial \tau}\left(k \rho u y^{2j} \tau^{-j} \frac{\partial T}{\partial \tau}\right) + \frac{\mu \rho^2 u^2 y^{2j}}{(1 + j)^2 \tau^{2j}}\left(\frac{\partial u}{\partial \tau}\right)^2 \end{aligned}\right\} \tag{5}$$

Nondimensional variables can now be introduced:

$$\left.\begin{aligned} \tilde{\xi} &= (1 + j)^{-2} \int_{x_i}^{x} \frac{1}{r_b} \frac{dx}{R_e} \\ \tilde{\tau} &= \frac{\tau}{r_b\left(\rho_e u_e\right)^{1/(1+j)}} \end{aligned}\right\} \tag{6}$$

and

$$\bar{u} = \frac{u}{u_e} \qquad \bar{\mu} = \frac{\mu}{\mu_e}$$

$$\bar{T} = \frac{T}{T_e} \qquad \bar{C} = \frac{\rho\mu}{\rho_e\mu_e}$$

$$\bar{\rho} = \frac{\rho}{\rho_e} \qquad \bar{y} = \frac{y}{r_b}$$

where x_i is the initial value of x, $R_e = \rho_e u_e r_b/\mu_e$, and r_b is a characteristic body dimension. The momentum and energy equations become

$$\bar{C}\bar{u}\left(\frac{\bar{y}}{\bar{\tau}}\right)^{2j}\bar{u}_{\bar{\tau}\bar{\tau}} + \bar{C}\bar{u}_{\bar{\tau}}\left\{j\left(\frac{4}{\bar{\rho}\bar{\tau}} - \frac{\bar{u}\bar{y}^2}{\bar{\tau}^3}\right) + \left(\frac{\bar{y}}{\bar{\tau}}\right)^{2j}\left[\bar{u}_{\bar{\tau}} + \bar{u}\left(\ln \bar{C}\right)_{\bar{\tau}}\right]\right.$$

$$\left. + \underline{\frac{\bar{\tau}}{j+1}\frac{1 - M_e^2}{\bar{C}}\left(\ln u_e\right)_{\bar{\xi}}}\right\} - \bar{u}_{\bar{\xi}} = \left(\bar{u} - \frac{1}{\bar{\rho}\bar{u}}\right)\left(\ln u_e\right)_{\bar{\xi}} \tag{7}$$

and

$$\frac{\bar{C}\bar{u}}{\sigma}\left(\frac{\bar{y}}{\bar{\tau}}\right)^{2j}T_{\bar{\tau}\bar{\tau}} + \frac{\bar{C}}{\sigma}\bar{T}_{\bar{\tau}}\left\{j\left(\frac{4}{\bar{\rho}\bar{\tau}} - \frac{\bar{y}^2\bar{u}}{\bar{\tau}^3}\right) + \left(\frac{\bar{y}}{\bar{\tau}}\right)^{2j}\left[\bar{u}_{\bar{\tau}} + \bar{u}\left(\ln\frac{\bar{C}}{\sigma}\right)_{\bar{\tau}}\right]\right.$$

$$\left. + \underline{\frac{\sigma}{\bar{C}}\bar{\tau}\frac{1 - M_e^2}{1 + j}\left(\ln u_e\right)_{\bar{\xi}}}\right\} - \bar{T}_{\bar{\xi}} = -(\gamma - 1)M_e^2\left[\bar{C}\bar{u}\left(\frac{\bar{y}}{\bar{\tau}}\right)^{2j}\left(\bar{u}_{\bar{\tau}}\right)^2\right] \tag{8}$$

where the subscripts $\bar{\tau}$ and $\bar{\xi}$ denote differentiation with respect to $\bar{\tau}$ and $\bar{\xi}$, respectively. The initial and boundary conditions for the wake are

$$\bar{u}(0,\bar{\tau}) = \bar{u}_i(\bar{\tau}) \qquad \bar{T}(0,\bar{\tau}) = \bar{T}_i(\bar{\tau})$$

$$u_{\bar{\tau}}(\bar{\xi},0) = \bar{T}_{\bar{\tau}}(\bar{\xi},0) = 0 \qquad \lim_{\bar{\tau}\to\infty}\bar{u}(\bar{\xi},\bar{\tau}) = \lim_{\bar{\tau}\to\infty}\bar{T}(\bar{\xi},\bar{\tau}) = 1$$

At this point, these equations and the dependent and independent variables are now the same as those in reference 14 except for the additional underlined terms and the fact

that $\bar{\tau}_{\bar{x}}$ is not related to $\bar{\rho}\bar{v}$ as indicated in reference 14. Note that for flows with zero pressure gradient the underlined terms are identically zero, and in this case the analysis of reference 14 gives correct results. The modification of the program of reference 14 for the correct computation of flows with pressure gradients is quite straightforward; this modification was made by simply including the underlined terms in the transformed equations at the appropriate locations in the program. (Similar corrections for the species equation for flows with dissimilar gas mixing would occur.)

Turbulence models.- Equations (7) and (8) are applied to either laminar, turbulent, or intermittently turbulent flow by using transport models for the transport coefficients μ and σ. The turbulent-flux terms in the mean-flow equation are modeled by an eddy viscosity and a turbulent Prandtl number; that is,

$$\left.\begin{aligned} &\text{Turbulent shear stress} = \mu_T \frac{\partial u}{\partial y} \\ &\text{Turbulent heat flux} = \frac{\mu_T}{\sigma_T} \frac{\partial h}{\partial y} \end{aligned}\right\} \tag{9}$$

where σ_T is the turbulent Prandtl number. The intermittent nature of the viscous wake flow is accounted for by an intermittency factor γ_T so that the total shear stress (and correspondingly for the heat transfer) is

$$\text{Total shear stress} = \mu \frac{\partial u}{\partial y} = \left(\mu_l + \gamma_T \mu_T\right) \frac{\partial u}{\partial y} \tag{10}$$

where γ_T is 1 for fully turbulent flow and 0 for fully laminar flow. Since $\sigma = c_p \mu / k$,

$$\frac{\sigma}{\sigma_l} = \frac{1 + \gamma_T \dfrac{\mu_T}{\mu_l}}{1 + \gamma_T \dfrac{\mu_T}{\mu_l} \dfrac{\sigma_l}{\sigma_T}}$$

For simplicity, the laminar Prandtl number σ_l was assumed to be equal to the turbulent Prandtl number σ_T, so that $\sigma = \sigma_T$. An approximation made by Townsend and given by Hinze in reference 16 for the distribution of the intermittency was assumed herein for all calculations:

$$\gamma_T = \left[1 + C_\gamma \left(\frac{y}{y_{1/2}}\right)^4\right]^{-1} \tag{11}$$

where $y_{1/2}$ is the velocity-defect half-width of the wake $\left(\text{i.e., where } u(y) - u_o = \frac{u_e - u_o}{2}\right)$. The constant C_γ was taken as 0.142, a value which gives close agreement with the intermittency distribution given in reference 17. Demetriades (ref. 18) has measured the variation of γ_T in the wake of a thin plate at a Mach number of 3 and has found the same dependence of γ_T upon y as in equation (11) and nearly the same value of C_γ.

Different formulations for the eddy viscosity (representative of those found in the literature) were examined. Calculations were made by assuming an eddy viscosity proportional to the velocity defect in the wake; that is,

$$\mu_T = K_u \rho_e y_{1/2}(u_e - u_o) \tag{12}$$

or, proportional to an integral of the mass-flow defect,

$$\mu_T = K_m \int_0^\infty (\rho_e u_e - \rho u)dy \tag{13}$$

The first formulation is the classical Prandtl hypothesis (ref. 19) and the latter has been suggested by Schetz (ref. 20). Both methods predict a constant eddy viscosity across the wake.

In addition to these models, calculations were made on the basis of a mixing-length type of formulation for the eddy viscosity

$$\mu_T = \rho l^2 \sqrt{\left(\frac{\partial u}{\partial y}\right)^2 + l_1^2 \left(\frac{\partial^2 u}{\partial y^2}\right)^2} \tag{14}$$

which has been suggested in the literature by Prandtl (ref. 19). The velocity-gradient term and the mixing length l are the usual quantities introduced in the typical approach for turbulent boundary layers, but the term proportional to the second derivative of the velocity was suggested by Prandtl to modify the usual mixing-length model which predicts vanishing eddy viscosity at the wake plane of symmetry, a result inconsistent with observations. In all calculations herein, it was assumed that $\left(l/y_{1/2}\right) = 0.32$ and $l = l_1$. Since $y_{1/2} \approx \frac{1}{4}\delta$ (the wake width), the variation of l chosen is nearly $l \approx 0.08\delta$, which is a good approximation for mixing lengths in the outer part of turbulent boundary layers (ref. 21). This value of $l/y_{1/2}$ is close to the value obtained by Schlichting in low-speed wakes (ref. 19).

Comparisons of predictions and experimental data.- Initial velocity and temperature profiles for the finite-difference calculations were obtained from the experimental data at

$x/t = 6.0$. The downstream development of the wake was computed using each of the turbulent transport models discussed previously, and one calculation was made assuming laminar transport. For the laminar transport properties, the assumptions $\sigma = 1.0$ and $\rho\mu = \rho_e\mu_e$ were made. Experimental and predicted velocity and temperature defects at the plane of symmetry (the maximum defects) are shown in figures 9(a) and 9(b). Edge conditions were obtained from the values computed at the edge of the viscous wake or just downstream of the wake shock for those stations where the viscous wake edge is not well defined (x/t less than about 5). The departure of the experimental data from the laminar calculation beyond the initial station is further evidence that transition to turbulent flow occurs in the wake upstream of $x/t = 6.0$.

Two calculations shown in figures 9(a) and 9(b) were performed with the modified mixing-length model: one calculation with $\sigma_T = \sigma_l = 1.0$ and the other with $\sigma_T = \sigma_l = 0.68$. The latter value equals the actual molecular Prandtl number for helium at the temperatures present in the wake. The Prandtl number assumption appears to have a measurable effect upon the temperature-defect variation but only a slight effect on the velocity defect. Although better results would probably occur for a value of σ_T between 0.68 and 1.0, either of the present calculations is considered to yield good predictions.

Calculations were made with the classical mixing-length theory $(l_1 = 0)$ and assuming still that $\left(l/y_{1/2}\right) = 0.32$, but the results were unrealistic. (See figs. 9(a) and 9(b).) Although the turbulent viscosity was as much as 30 times greater than the laminar viscosity, the calculations gave almost as slow relaxation (i.e., less mixing) of the velocity and temperature defects as that occurring in the laminar solution. This result was not expected, since the primary effect of the additional term in the modified mixing-length theory is to give nonzero values for the eddy viscosity at the plane of symmetry; elsewhere the eddy viscosity is not greatly changed. For the mixing-length theory, the rapid decrease of the eddy viscosity as y approaches zero apparently is difficult to accommodate in the solution. Schlichting (ref. 19) has pointed out that analyses of low-speed free shear layers using the classical mixing-length theory have the general property that discontinuities in u_{yy} occur in the solutions; for example u_{yy} becomes infinitely large at $y = 0$ in a wake. The unrealistic results obtained herein may be a manifestation of such a singularity. Schlichting (ref. 19) also states that the modified mixing-length theory is free of such difficulties.

Through appropriate choices of the constants in the eddy-viscosity formulations of the algebraically simpler models, Prandtl's hypothesis (velocity-defect model) and Schetz' model, good predictions of the maximum velocity and temperature defects could be obtained. (See figs. 9(a) and 9(b).) In the velocity-defect model, the value of K_u used was 0.036. Lees and Hromas proposed a velocity-defect model with $K_u = 0.040$ and a transformed wake thickness (ref. 22) instead of the velocity-defect half-width $y_{1/2}$ used herein. For the density ratios present in these experiments, these changes in the model

would not have large effects on the eddy-viscosity levels. In Schetz' model the value of K_m was 0.005; this value is an order of magnitude lower than the value recommended by Schetz, $K_m = 0.060$. (In an evaluation of axisymmetric jet mixing, Eggers (ref. 23) has similarly found Schetz' recommended constants too large by a factor of 6.) This model gave nearly the same solution as the velocity-defect model and for this reason will be omitted in later comparisons of theory and data.

Velocity and temperature distributions from the experiments and the computations are shown in figures 10(a) and 10(b). All the theoretical models gave solutions which yield good predictions of the velocity distributions. Because of the nearly identical velocity distributions, only the modified mixing-length theory $(\sigma_T = 1.0)$ is shown in figure 10(a). The temperature distributions (fig. 10(b)) do show some differences between the calculations. Again, as for the maximum temperature defects, the two calculations by the modified mixing-length theory indicate that improved calculations of the temperature distributions near $y = 0$ can be obtained for σ_T between the values shown. The velocity-defect model, although yielding good predictions of the maximum temperature defects, predicts temperature profiles which are slightly fuller than the experimental profiles as do the modified-mixing-length calculations. Nevertheless, all the calculations are considered to give good predictions.

The momentum thickness θ and displacement thickness δ^* of the wake are shown in figure 11. Also shown are the velocity-defect half-widths $y_{1/2}/t$. The increase in momentum thickness with x/t occurs because of the pressure gradient in the wake. To check the consistency of the data, the initial value of θ and the experimental values of δ^*, M_e, and dp_e/dx were used in the integral momentum equation (ref. 19) to calculate the momentum-thickness growth. The calculated variation (see fig. 11) agrees well with the experimental variation of θ with x. The generally good agreement of the data and the results of the finite-difference solutions would be expected in view of the close profile predictions previously discussed.

Turbulent transport models which give the eddy viscosity proportional to a velocity or mass-flow defect, such as the Prandtl hypothesis or Schetz' model, would be expected to be appropriate for a wake with near self-preserving similarity. Townsend (see ref. 18) has shown that at low speed a self-preserving similarity can be attained in zero-pressure-gradient wakes for Reynolds numbers, based on the wake momentum thickness, greater than 400. Demetriades has observed in a two-dimensional supersonic wake (ref. 18) that the self-preserving similarity of incompressible far wakes is also reached in compressible wakes. The Reynolds number based on momentum thickness at the initial station herein is $R_\theta \approx 800$. The question exists whether the magnitude of this Reynolds number is such that a self-preserving similarity can be established in the present wake with nonzero pressure gradient. It was of interest to determine whether similarity was approached in the present experiments.

An analysis of the admissible similar solutions, or the appropriate similarity variables, for compressible wakes with a pressure gradient (as described by eqs. (7) and (8)) was not attempted. Instead, similarity was investigated by using the similarity variables firmly established in the literature for wakes with zero pressure gradient (refs. 16 to 18) in the belief that the streamwise pressure gradient would have only a small effect on the appropriate variables. In figure 12 this approach is taken, and the velocity and temperature defects in the wake are shown divided by the corresponding maximum defects and plotted against the transverse coordinate y scaled by the half-width of the wake velocity defect $y_{1/2}$. The velocity-defect data display "similarity" and the correlation agrees closely with the results obtained by Townsend at low speeds. The temperature-defect data also display similarity even though the transverse coordinate is scaled by the *velocity-defect half-width.* (*Note that the low-speed velocity defect is also shown in the* temperature-defect correlation for comparison.) The degree of similarity shown is rather surprising in view of the results obtained by Demetriades (ref. 18), who finds that at $M_e = 3$ the wake of a flat plate does not attain self-preserving similarity until the distance from the virtual origin of the turbulence (see fig. 8) exceeds 1000θ. Herein the minimum value of θ is about 0.02t, and therefore, similarity would not be expected upstream of $x/t \approx 20$.

Although the present experiments contain pressure-gradient effects, it is of interest to determine the turbulent Reynolds number (ref. 18) defined for wake flows with zero pressure gradient as

$$R_T = 5 \frac{x - x_{vo}}{\theta} \left(\frac{u_e - u_o}{u_e} \right)^2 \tag{15}$$

where x_{vo} is the virtual origin of the turbulent wake. Using the linear curve fit downstream of transition in figure 8 and an average value of θ gives $R_T \approx 12.0$, which is comparable to the Demetriades (ref. 18) value, $R_T = 13.0$.

CONCLUDING REMARKS

Experiments have been performed to determine the flow in the turbulent wake produced by a two-dimensional wedge in hypersonic helium flow. From these experiments, mean-flow profiles were obtained and compared with finite-difference calculations of the subsequent wake development with various models inserted for the turbulent transport. The comparison of calculations and experimental data shows that by proper choice of empirical constants, the turbulent transport models that employ eddy-viscosity formulations based on velocity or mass-flow defects can yield accurate predictions of hypersonic, turbulent wake flow including the effects of pressure gradients. However, the classical

mixing-length theory was found to yield unrealistic results when used in the finite-difference calculations. When the classical mixing-length theory is modified to include a second-derivative term in the eddy-viscosity formulation, the difficulties of the classical mixing-length theory are not encountered. In fact, the modified mixing-length theory yields excellent predictions of the wake development when the mixing-length constants in the theory are chosen to be consistent with turbulent-boundary-layer results. This link to the results of turbulent-boundary-layer theory is a strong point in favor of the modified mixing-length theory over the defect-type models for which the choice of empirical constants is apparently flow dependent.

The experimental data displayed similarity when velocity and temperature defects were scaled by the maximum defects and the transverse coordinate was scaled by the velocity-defect half-width. On the basis of the results of previous studies, this similarity would not be expected in the region investigated.

Langley Research Center,
National Aeronautics and Space Administration,
Hampton, Va., October 6, 1972.

REFERENCES

1. Lykoudis, Paul S.: A Review of Hypersonic Wake Studies. AIAA J. vol. 4, no. 4, Apr. 1966, pp. 577-590.

2. Korkegi, Robert H.: Survey of Viscous Interactions Associated With High Mach Number Flight. AIAA J., vol. 9, no. 5, May 1971, pp. 771-784.

3. Arrington, James P.; Joiner, Roy C., Jr.; and Henderson, Arthur, Jr.: Longitudinal Characteristics of Several Configurations at Hypersonic Mach Numbers in Conical and Contoured Nozzles. NASA TN D-2489, 1964.

4. Nicoll, K. M.: Investigation of the Laminar Boundary Layer on a Flat Plate in Helium Using the Crocco Method. ARL 62-345, U.S. Air Force, May 1962.

5. Behrens, Wilhelm: Viscous Interaction Effects on a Static Pressure Probe at $M = 6$. AIAA J., vol. 1, no. 12, Dec. 1963, pp. 2864-2866.

6. Chang, Paul K.: Separation of Flow. Pergamon Press, Inc., c.1970.

7. Olsson, G. R.; and Messiter, A. F.: Hypersonic Laminar Boundary Layer Approaching the Base of a Slender Body. AIAA J., vol. 7, no. 7, July 1969, pp. 1261-1267.

8. Batt, Richard George: Experimental Investigation of Wakes Behind Two-Dimensional Slender Bodies at Mach Number Six. Ph. D. Thesis, California Inst. Technol., 1967.

9. Wagner, R. D., Jr.; Maddalon, D. V.; and Weinstein, L. M.: Influence of Measured Freestream Disturbances on Hypersonic Boundary-Layer Transition. AIAA J., vol. 8, no. 9, Sept. 1970, pp. 1664-1670.

10. Demetriades, Anthony: Hot-Wire Measurements in the Hypersonic Wakes of Slender Bodies. AIAA J., vol. 2, no. 2, Feb. 1964, pp. 245-250.

11. Demetriades, Anthony: Observations on the Transition Process of Two-Dimensional Supersonic Wakes. AIAA J., vol. 9, no. 11, Nov. 1971, pp. 2128-2134.

12. Behrens, Wilhelm; Lewis, John E.; and Webb, Wilmot H.: Transition and Turbulence Phenomena in Supersonic Wakes of Wedges. AIAA J., vol. 9, no. 10, Oct. 1971, pp. 2083-2084.

13. Laufer, John: Aerodynamic Noise in Supersonic Wind Tunnels. J. Aerosp. Sci., vol. 28, no. 9, Sept. 1961, pp. 685-692.

14. Sinha, Ram; Fox, Herbert; and Weinberger, Lawrence: An Implicit Finite Difference Solution for Jet and Wake Problems. Pt. I: Analysis and Test Cases. ARL 70-0025, U.S. Air Force, Feb. 1970. (Available from DDC as AD 707 865.)

15. Zakkay, Victor; and Fox, Herbert: An Experimental and Theoretical Investigation of the Turbulent Far Wake. AIAA J., vol. 5, no. 3, Mar. 1967, pp. 568-574.

16. Hinze, J. O.: Turbulence. McGraw-Hill Book Co., Inc., 1959.

17. Lin, C. C., ed.: Turbulent Flows and Heat Transfer. Princeton Univ. Press, 1959.

18. Demetriades, A.: Compilation of Numerical Data on the Mean Flow From Compressible Turbulent Wake Experiments. Publ. No. U-4970, Philco-Ford Corp., Oct. 1, 1971.

19. Schlichting, Hermann (J. Kestin, transl.): Boundary-Layer Theory. Sixth ed., McGraw-Hill Book Co., Inc., 1968.

20. Schetz, Joseph A.: Some Studies of the Turbulent Wake Problem. Astronaut. Acta, vol. 16, no. 2, Feb. 1971, pp. 107-117.

21. Harvey, William D.; Bushnell, Dennis M.; and Beckwith, Ivan E.: Fluctuating Properties of Turbulent Boundary Layers for Mach Numbers up to 9. NASA TN D-5496, 1969.

22. Lees, Lester; and Hromas, Leslie: Turbulent Diffusion in the Wake of a Blunt-Nosed Body at Hypersonic Speeds. J. Aerosp. Sci., vol. 29, no. 8, Aug. 1962, pp. 976-993.

23. Eggers, James M.: Turbulent Mixing of Coaxial Compressible Hydrogen-Air Jets. NASA TN D-6487, 1971.

TABLE I.- EXPERIMENTAL VELOCITY AND TEMPERATURE RATIOS

$x/t = 6.0$; $M_e = 5.15$; $T_{t,e} = 93.4^{\circ}$ C; $u_e = 1850 \frac{m}{s}$; $\frac{p_e}{p_\infty} = 9.19$		
y/t	u/u_e	T/T_e
0	0.8524	2.906
.011	.8524	2.906
.042	.8598	2.816
.073	.8692	2.673
.105	.8827	2.489
.136	.8975	2.287
.163	.9138	2.048
.192	.9269	1.867
.225	.9445	1.678
.253	.9614	1.458
.320	.9820	1.252
.380	.9948	1.090
.410	.9966	1.059
.450	.9984	1.037
.510	1.0000	1.000

$x/t = 8.98$; $M_e = 5.69$; $T_{t,e} = 94.7^{\circ}$ C; $u_e = 1868 \frac{m}{s}$; $\frac{p_e}{p_\infty} = 8.57$		
y/t	u/u_e	T/T_e
0.004	0.8968	2.535
.036	.8968	2.535
.071	.9025	2.419
.106	.9076	2.319
.140	.9168	2.177
.180	.9274	2.028
.240	.9516	1.679
.320	.9744	1.404
.390	.9875	1.211
.480	.9947	1.104
.560	.9968	1.057
.670	.9981	1.026
.790	.9987	1.009
.900	1.0000	1.000

$x/t = 10.0$; $M_e = 5.79$; $T_{t,e} = 93.4^{\circ}$ C; $u_e = 1872 \frac{m}{s}$; $\frac{p_e}{p_\infty} = 8.30$		
y/t	u/u_e	T/T_e
0.011	0.9061	2.448
.040	.9088	2.380
.090	.9121	2.317
.140	.9176	2.186
.180	.9325	1.944
.230	.9439	1.789
.280	.9601	1.582
.360	.9799	1.337
.440	.9898	1.195
.520	.9951	1.109
.600	.9973	1.066
.740	.9990	1.029
.840	.9993	1.016
.980	1.0000	1.000
1.060	1.0000	1.003

$x/t = 12.0$; $M_e = 5.95$; $T_{t,e} = 91.2^{\circ}$ C; $u_e = 1874 \frac{m}{s}$; $\frac{p_e}{p_\infty} = 7.69$		
y/t	u/u_e	T/T_e
0	0.9177	2.295
.010	.9177	2.290
.030	.9180	2.280
.084	.9208	2.225
.170	.9290	2.030
.260	.9452	1.764
.350	.9649	1.493
.440	.9821	1.274
.540	.9934	1.119
.640	.9972	1.066
.740	.9981	1.049
.840	.9988	1.029
.940	.9998	1.010
1.040	1.0000	1.000

$x/t = 14.0$; $M_e = 6.11$; $T_{t,e} = 93.4^{\circ}$ C; $u_e = 1877 \frac{m}{s}$; $\frac{p_e}{p_\infty} = 7.03$		
y/t	u/u_e	T/T_e
0	0.9219	2.302
.010	.9250	2.300
.040	.9230	2.240
.105	.9272	2.204
.196	.9348	2.044
.260	.9427	1.868
.380	.9624	1.548
.490	.9813	1.306
.640	.9943	1.122
.810	.9954	1.060
.980	.9982	1.038
1.130	.9990	1.015
1.330	1.0000	1.009
1.450	1.0000	1.000

$x/t = 16.94$; $M_e = 6.59$; $T_{t,e} = 93.2^{\circ}$ C; $u_e = 1890 \frac{m}{s}$; $\frac{p_e}{p_\infty} = 6.00$		
y/t	u/u_e	T/T_e
0	0.9300	2.120
.013	.9379	2.116
.038	.9390	2.100
.106	.9404	2.050
.201	.9447	1.927
.280	.9516	1.788
.360	.9609	1.604
.450	.9724	1.441
.540	.9825	1.297
.630	.9901	1.191
.730	.9950	1.128
.830	.9970	1.082
.930	.9980	1.060
1.030	.9988	1.035
1.140	.9993	1.023
1.240	.9996	1.009
1.360	1.0000	1.000
1.500	1.0004	.992

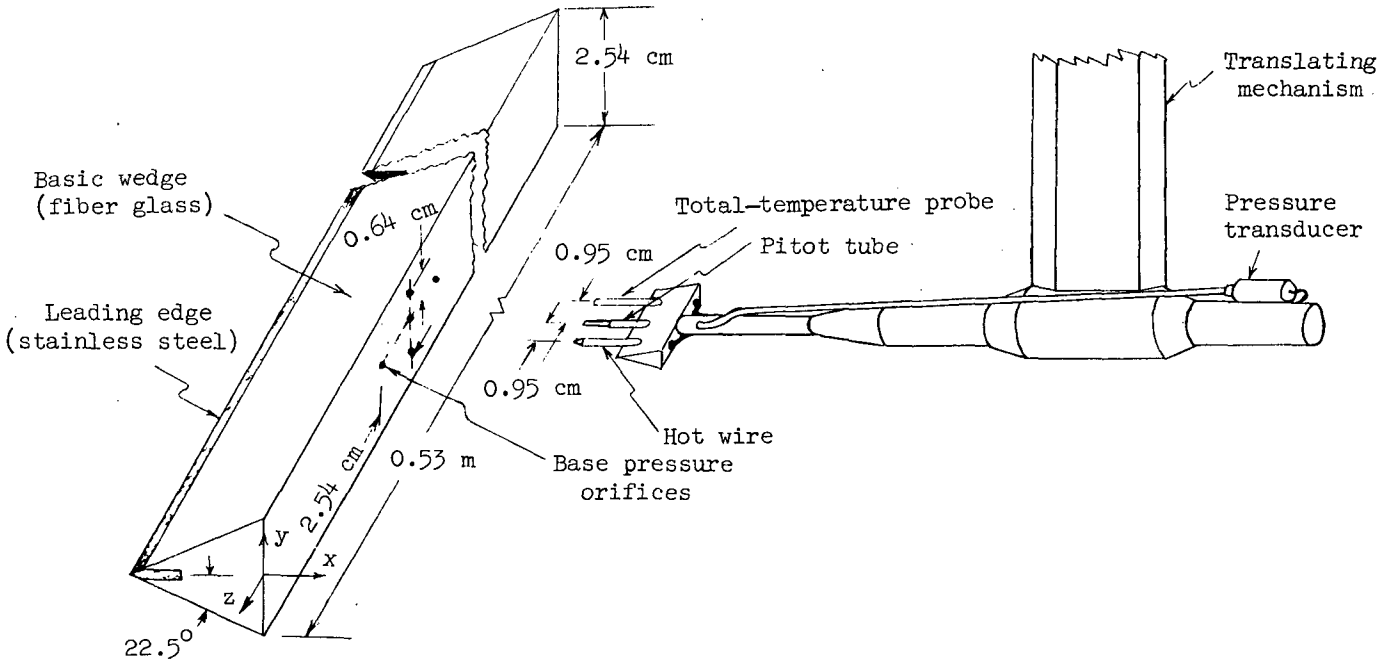

Figure 1.- Test model and survey rake.

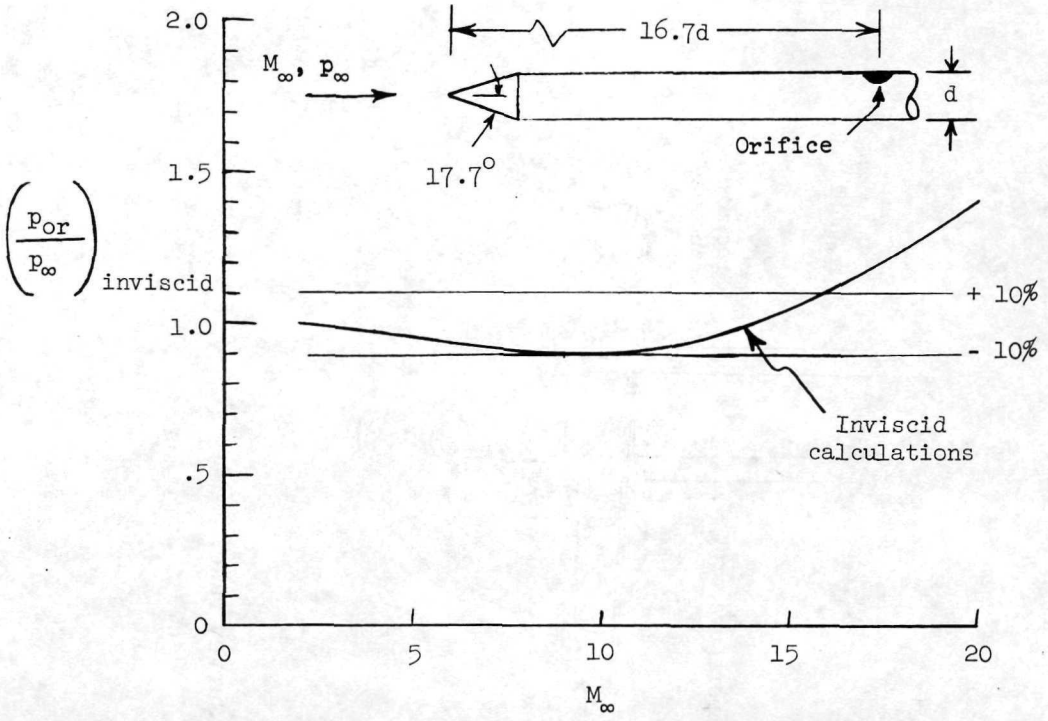

Figure 2.- Features of static-pressure probe.

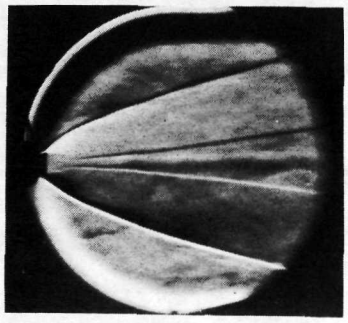

(a) Schlieren photograph.

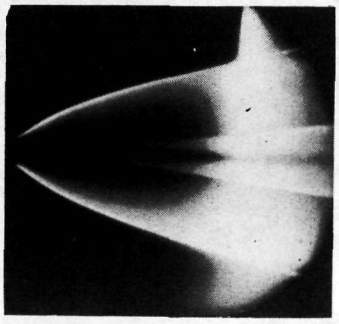

L-72-6530

(b) Electron-beam photograph.

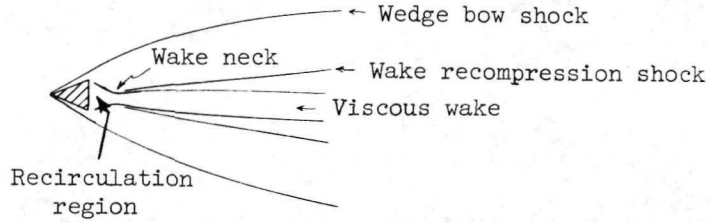

(c) Wake nomenclature.

Figure 3.- Flow visualization.

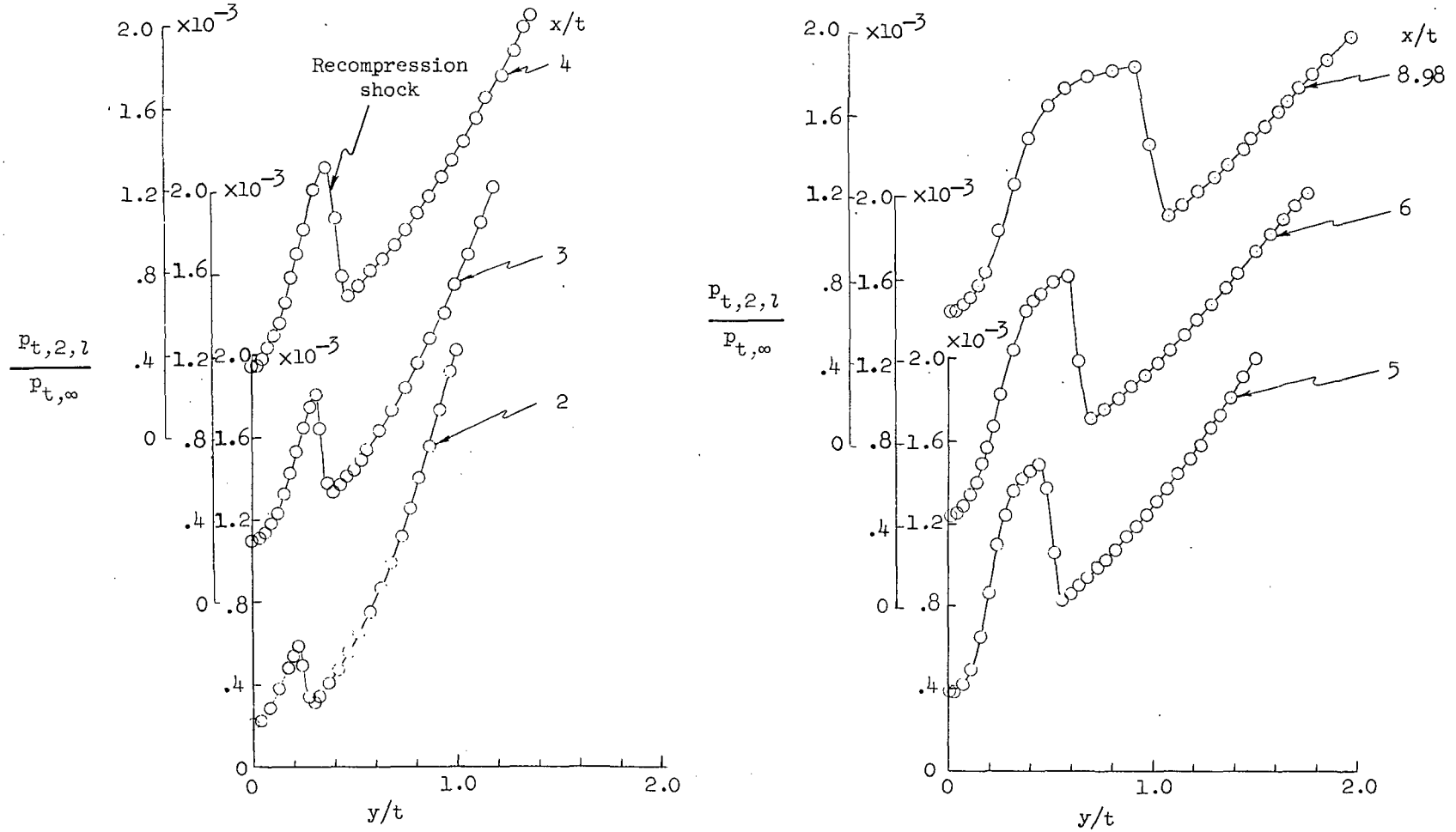

Figure 4.- Pitot-pressure distribution in wake of 22.5^{o} half-angle wedge. $M_{\infty} = 20.4$; $R_{\infty} = 3.4 \times 10^{5}$.

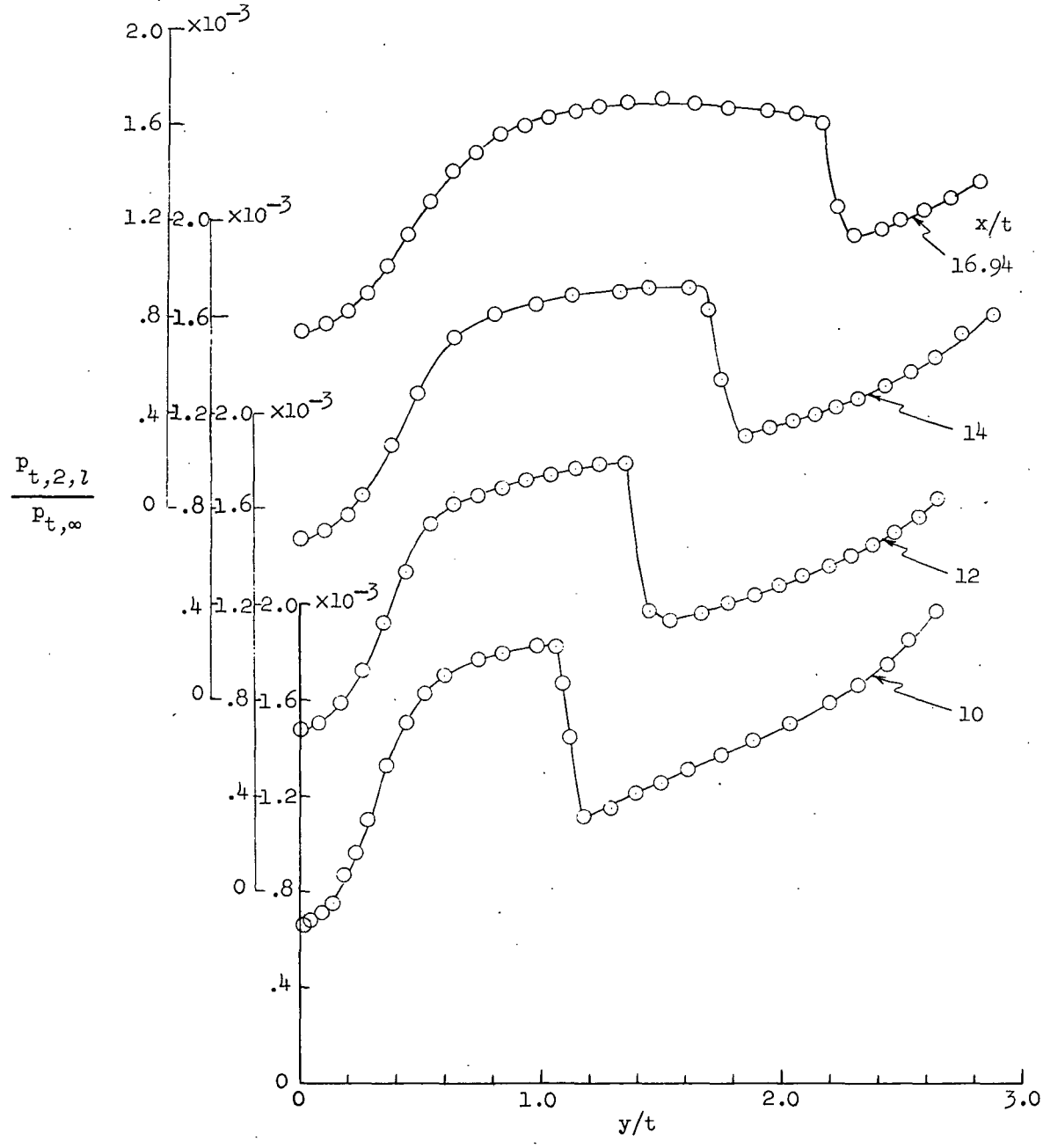

Figure 4.- Concluded.

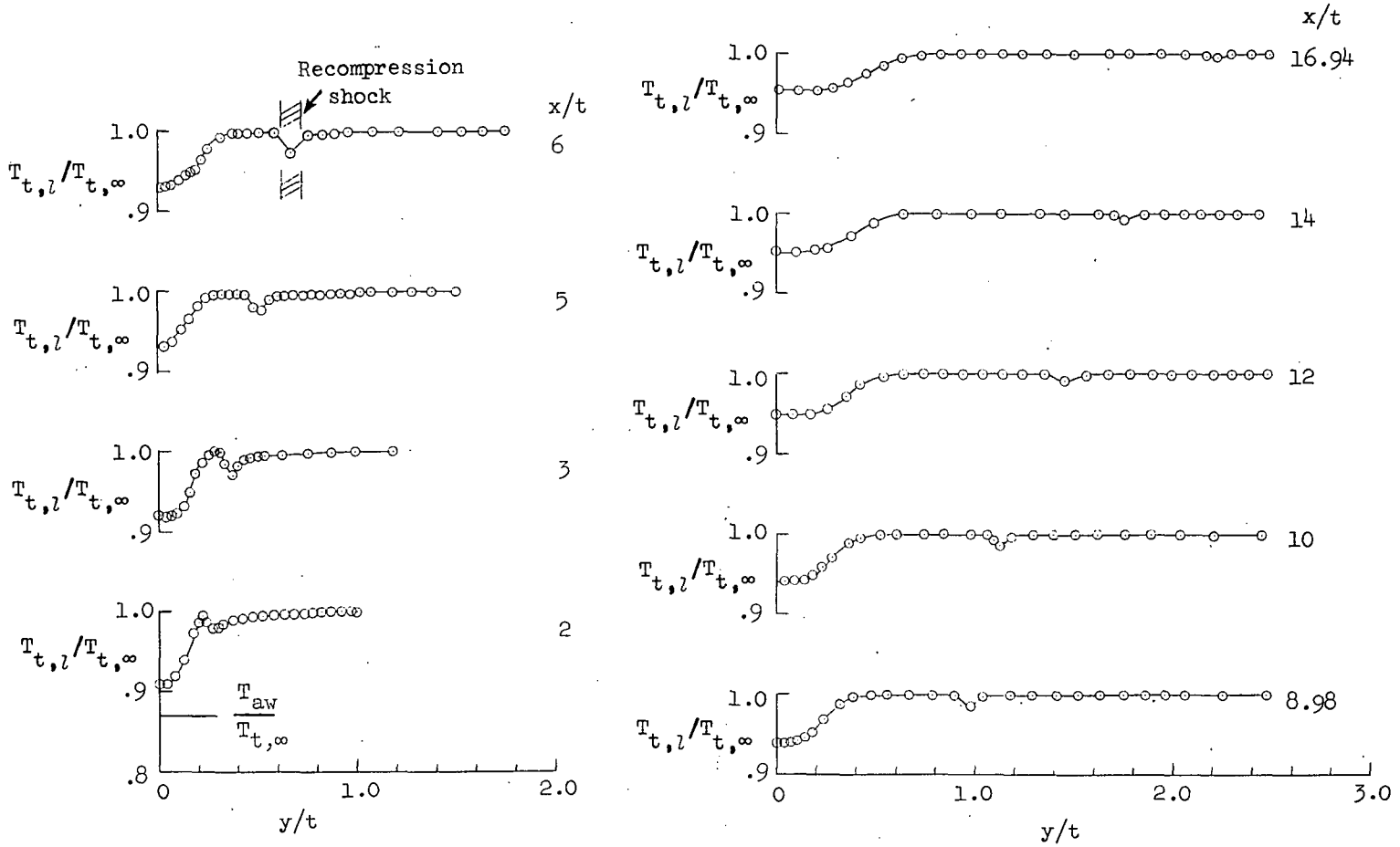

Figure 5.- Total-temperature distributions in wake of 22.5° half-angle wedge. $M_\infty = 20.4$; $R_\infty = 3.4 \times 10^5$.

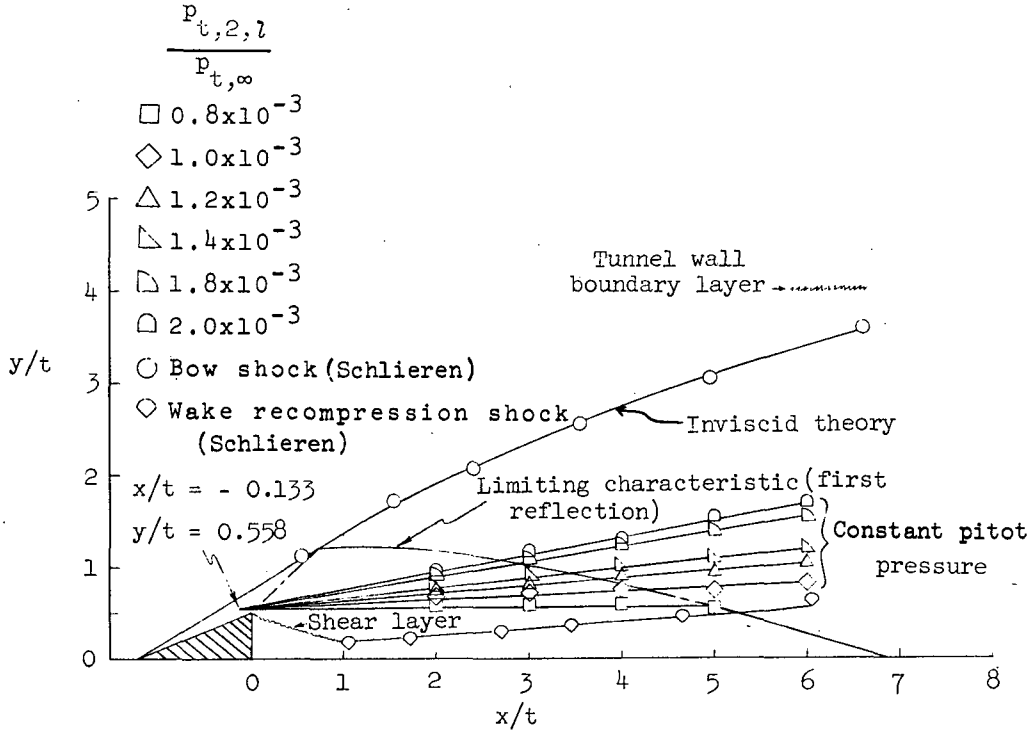

Figure 6.- Lines of constant pitot pressure. $M_\infty = 20.4$; $R_\infty = 3.4 \times 10^5$.

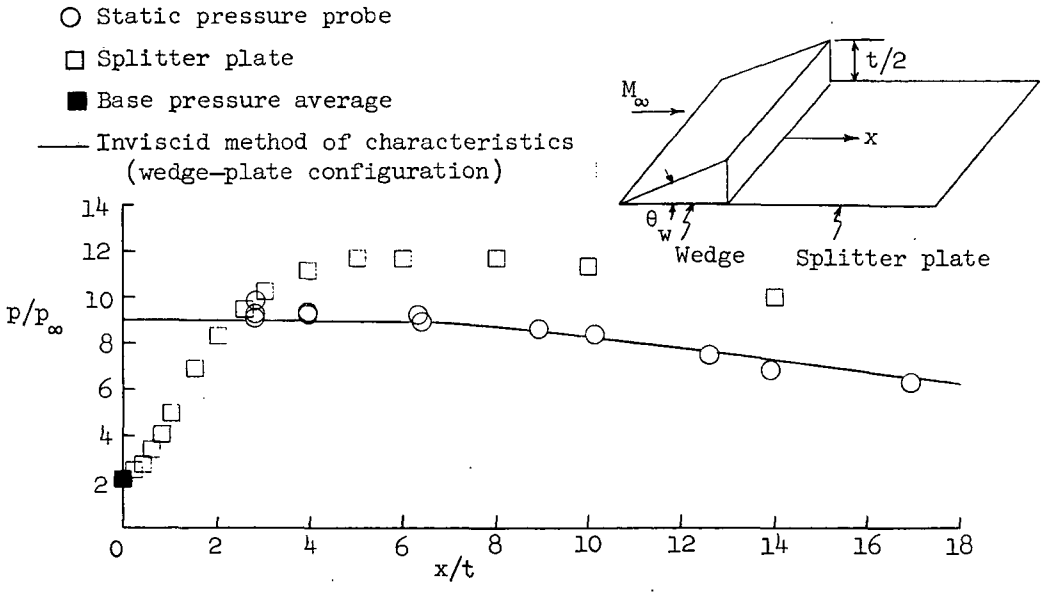

Figure 7.- Static-pressure distribution in wake and on splitter plate.

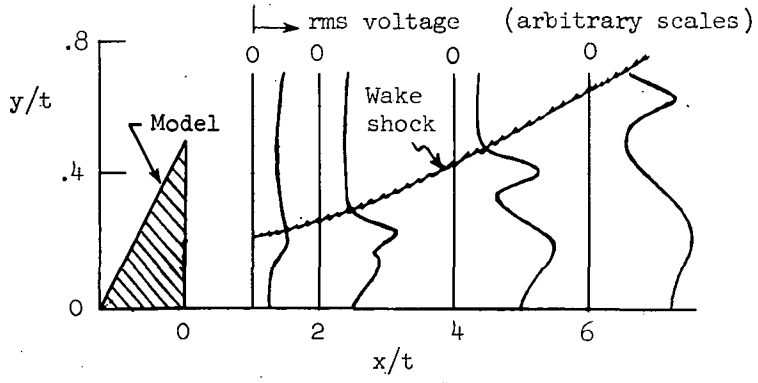

(a) rms voltage profiles.

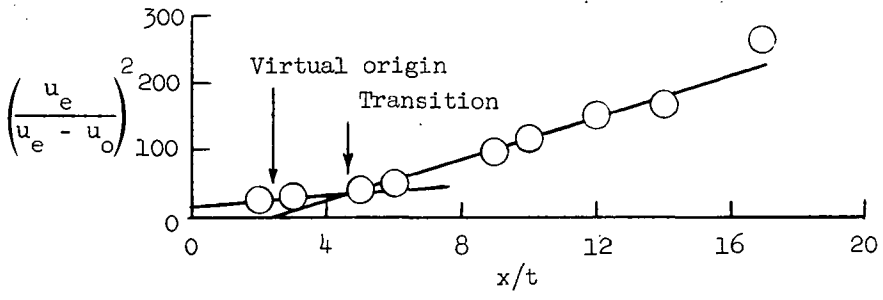

(b) Velocity defects.

Figure 8.- Transition detection in wake of 22.5° half-angle wedge. $M_\infty = 20.4$; $R_\infty = 3.4 \times 10^5$.

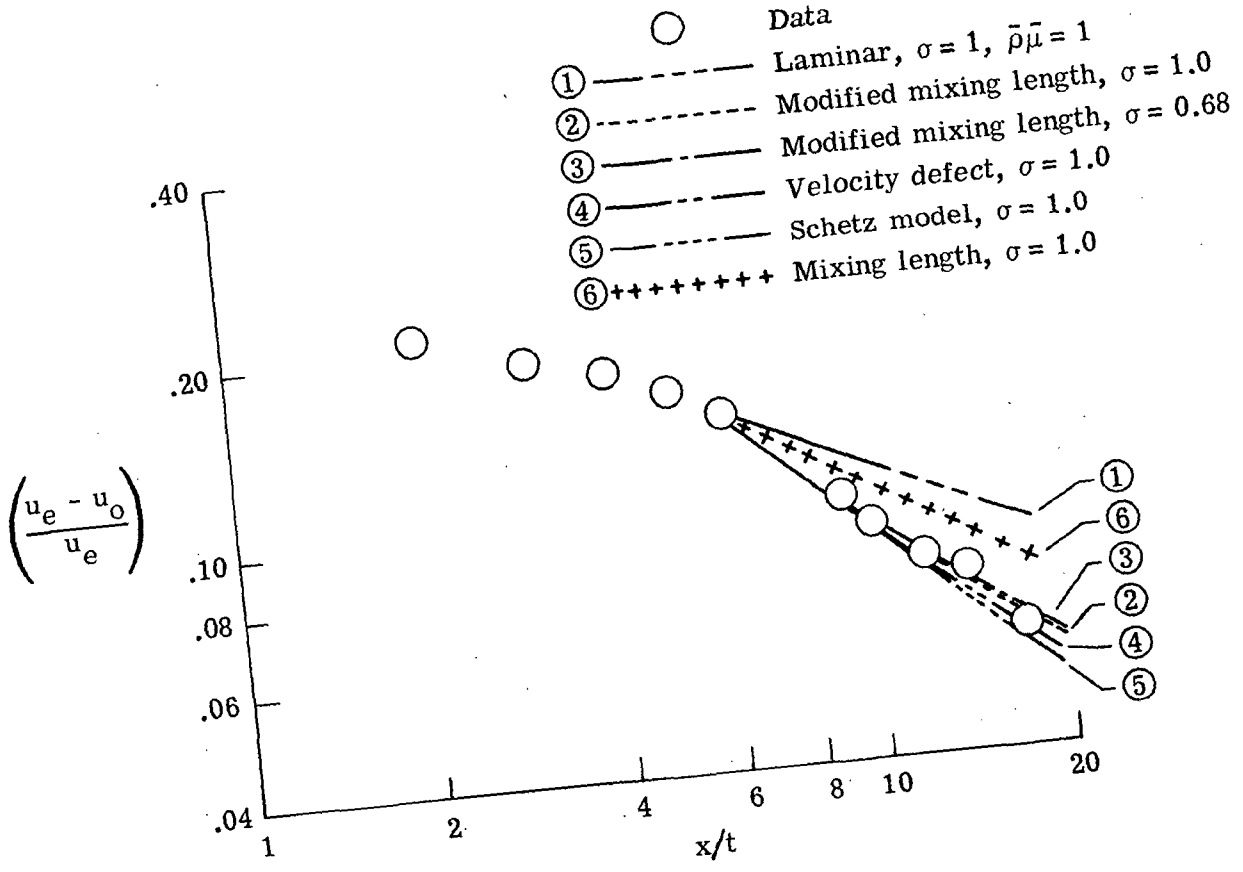

(a) Maximum velocity defects.

Figure 9.- Maximum temperature and velocity defects.

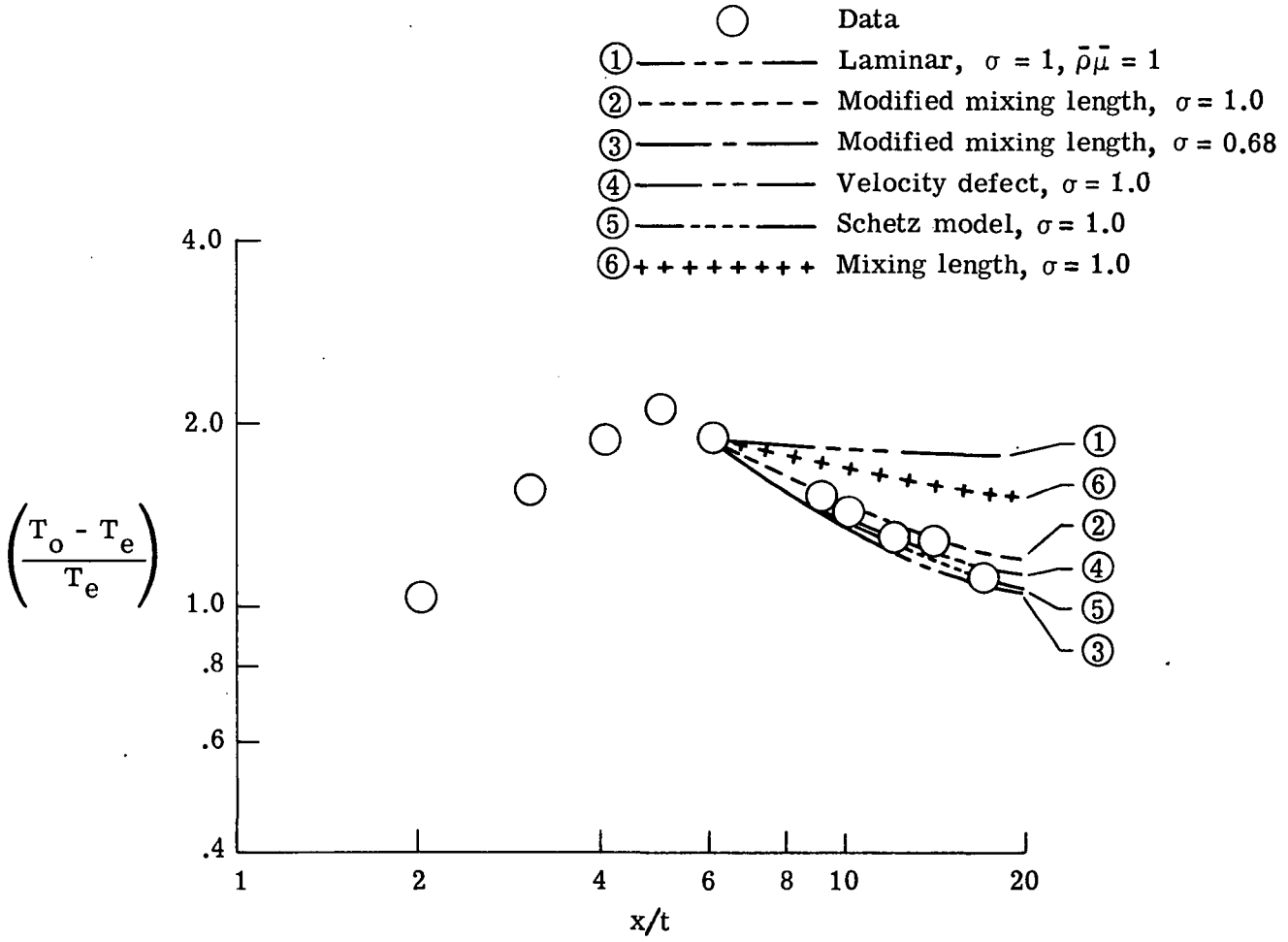

(b) Maximum temperature defects.

Figure 9.- Concluded.

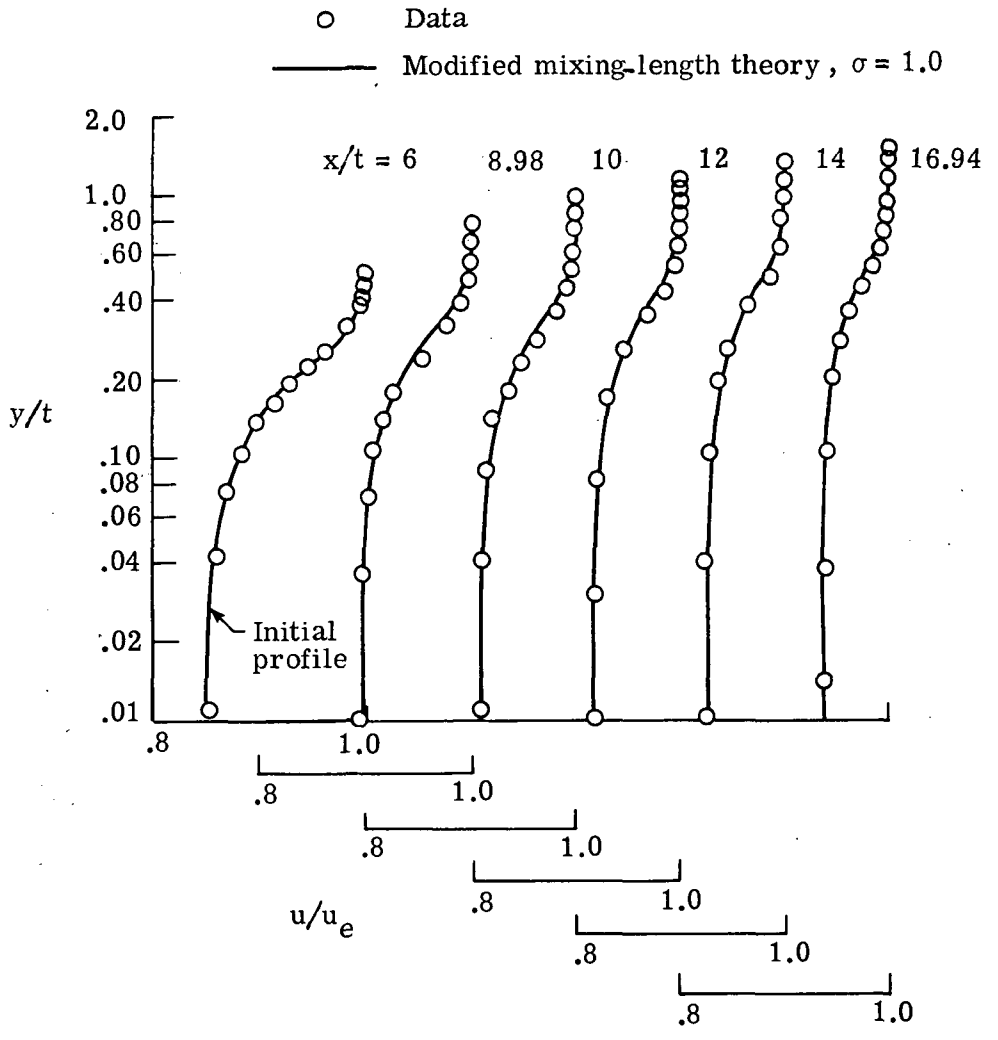

(a) Velocity profiles.

Figure 10.- Comparisons of computations and data.

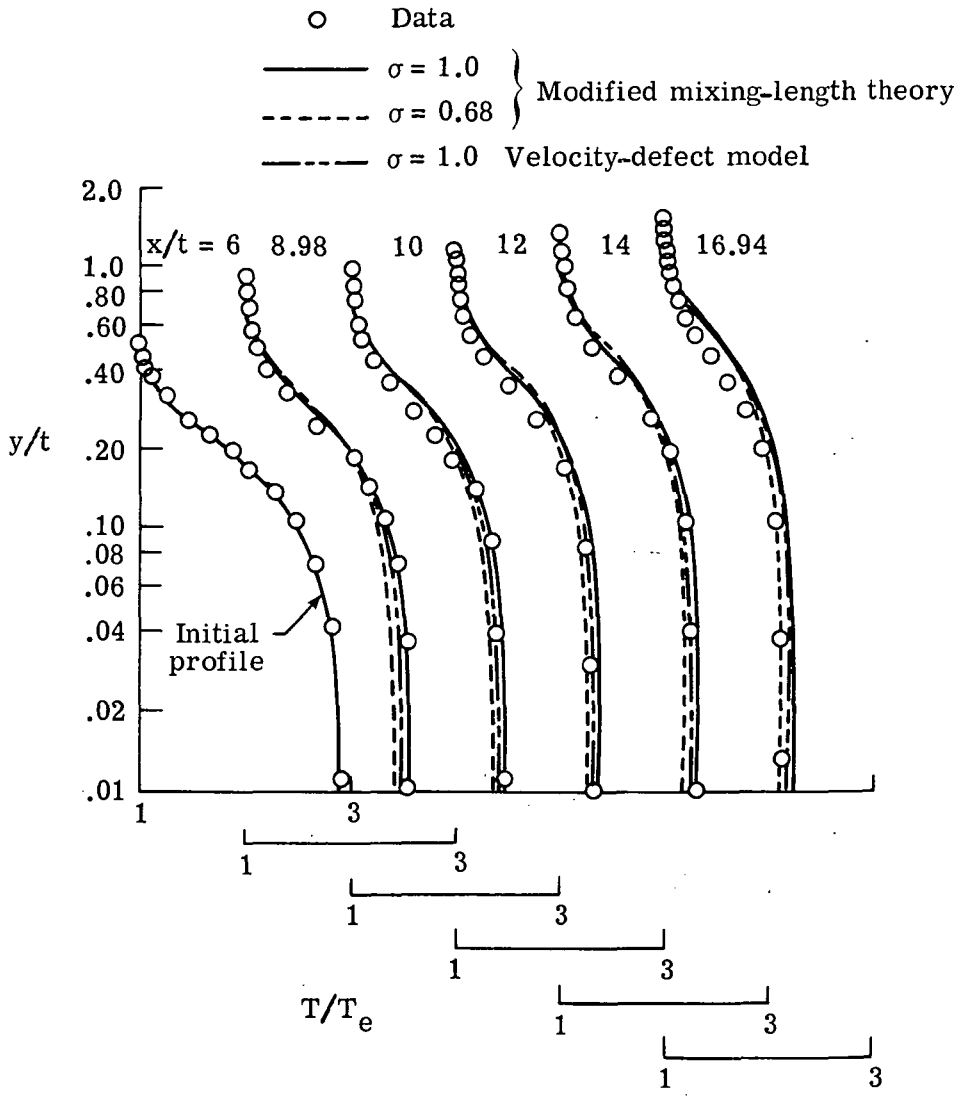

(b) Temperature profiles.

Figure 10.- Concluded.

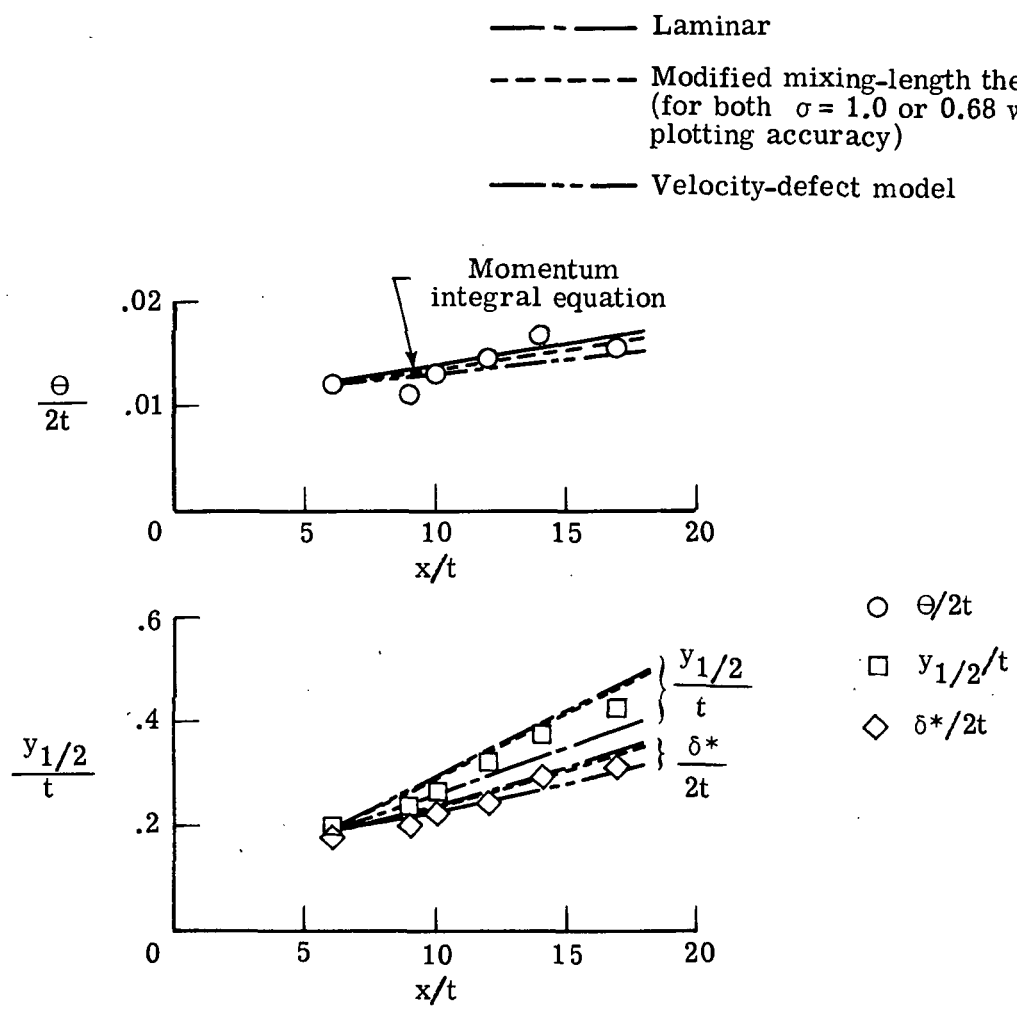

Figure 11.- Wake integral properties.

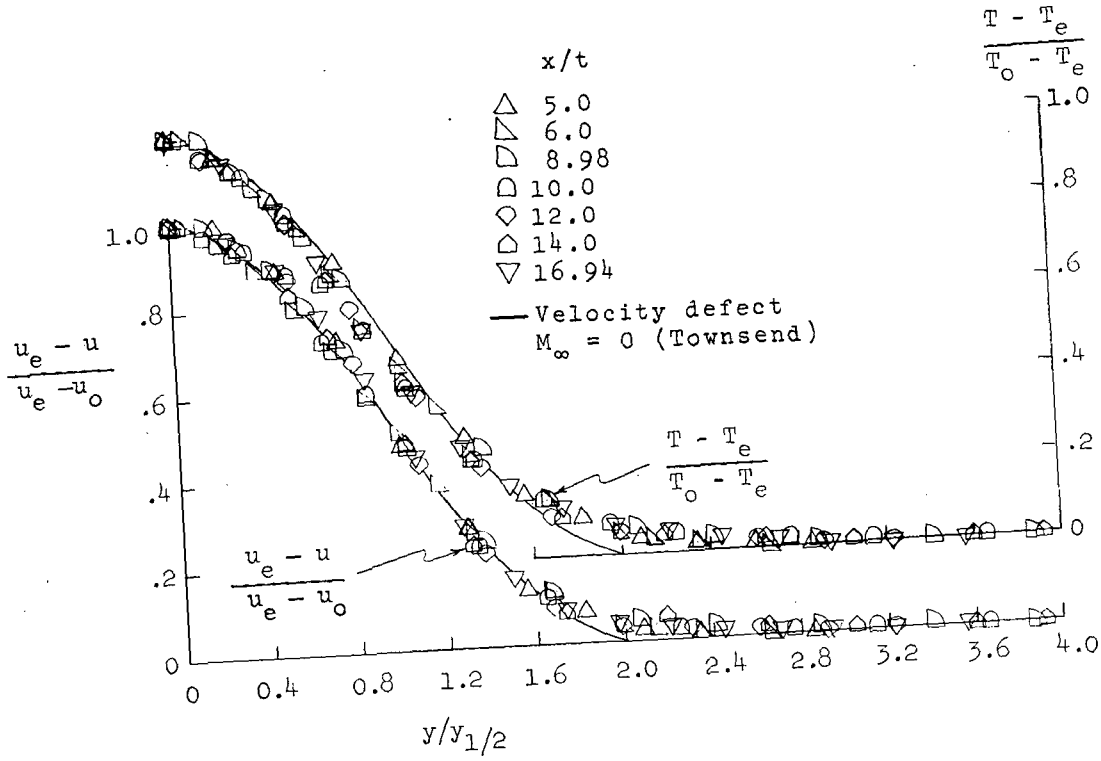

Figure 12.- Correlations of velocity and temperature defects.

NASA-Langley, 1972 — 12 L-8158

NATIONAL AERONAUTICS AND SPACE ADMINISTRATION
WASHINGTON, D.C. 20546

OFFICIAL BUSINESS
PENALTY FOR PRIVATE USE $300

SPECIAL FOURTH-CLASS RATE BOOK

POSTAGE AND FEES PAID
NATIONAL AERONAUTICS AND SPACE ADMINISTRATION
451

U.S.MAIL

POSTMASTER: If Undeliverable (Section 158 Postal Manual) Do Not Return

"The aeronautical and space activities of the United States shall be conducted so as to contribute . . . to the expansion of human knowledge of phenomena in the atmosphere and space. The Administration shall provide for the widest practicable and appropriate dissemination of information concerning its activities and the results thereof."

—NATIONAL AERONAUTICS AND SPACE ACT OF 1958

NASA SCIENTIFIC AND TECHNICAL PUBLICATIONS

TECHNICAL REPORTS: Scientific and technical information considered important, complete, and a lasting contribution to existing knowledge.

TECHNICAL NOTES: Information less broad in scope but nevertheless of importance as a contribution to existing knowledge.

TECHNICAL MEMORANDUMS: Information receiving limited distribution because of preliminary data, security classification, or other reasons. Also includes conference proceedings with either limited or unlimited distribution.

CONTRACTOR REPORTS: Scientific and technical information generated under a NASA contract or grant and considered an important contribution to existing knowledge.

TECHNICAL TRANSLATIONS: Information published in a foreign language considered to merit NASA distribution in English.

SPECIAL PUBLICATIONS: Information derived from or of value to NASA activities. Publications include final reports of major projects, monographs, data compilations, handbooks, sourcebooks, and special bibliographies.

TECHNOLOGY UTILIZATION PUBLICATIONS: Information on technology used by NASA that may be of particular interest in commercial and other non-aerospace applications. Publications include Tech Briefs, Technology Utilization Reports and Technology Surveys.

Details on the availability of these publications may be obtained from:

SCIENTIFIC AND TECHNICAL INFORMATION OFFICE

NATIONAL AERONAUTICS AND SPACE ADMINISTRATION

Washington, D.C. 20546